11-28-2017

A Preliminary Study of Conductive Filaments Printed Via Fused Filament Fabrication

Smruti Ranjan Sahoo
sxs7577@rit.edu

R.I.T

A Preliminary Study of Conductive Filaments Printed Via Fused Filament Fabrication

By
Smruti Ranjan Sahoo

A Thesis submitted in partial fulfillment of the requirement for the Degree of Masters of Science in Industrial and Systems Engineering

Department of Industrial and Systems Engineering
11/28/17

Department of Industrial and Systems Engineering
Kate Gleason College of Engineering
Rochester Institute of Technology
Rochester, New York

A Preliminary Study of Conductive Filaments Printed Via Fused Filament Fabrication

The Master of Science Degree thesis of Smruti Ranjan Sahoo has been examined and approved by the thesis committee as satisfactory for the thesis requirement for the Master of Science Degree in Industrial and Systems Engineering

Approved By:

Dr. Denis Cormier, Thesis Advisor
Department of Industrial and Systems Engineering

Dr. Ronald Aman, Committee Member
Department of Industrial and Systems Engineering

Abstract

Initially used as a prototyping tool for designers, additive manufacturing, also popularly known as 3D printing, has become an advanced process for manufacturing usable parts. This technology is expanding rapidly into a wide number of areas, such as electronic device fabrication, wearable electronics, biometric devices etc. It is especially useful for fabricating electronic devices, as it is possible to additively manufacture electrical traces within mechanical components simultaneously in a single operation cycle. This research specifically explores 3D printing using conductive feedstock materials with the fused filament extrusion (FFE) process. Commercially available conductive silver nanoparticle ink and graphene based polylactic acid (PLA) were printed using micro-extrusion and FFE techniques. Printing process parameters were adjusted using statistical analysis tools to enhance the conductivity of the printed conductive materials. A statistical analysis was also conducted on the samples to assess the impact of trace length, printing orientation, and aspect ratio on electrical conductivity.

Acknowledgements

This has been a fun and memorable experience working on my research. I would like to extend my deepest gratitude to my adviser Dr. Denis Cormier for the opportunity to work on such an exciting project. I had a great experience working on the project, which was a great learning experience, not just limited to academics but work ethics and dedication towards a goal. Dr. Cormier had great dedication and impact in this research area, yet he is the humblest person I met.

I would also like to thank my secondary adviser Dr. Ronald Aman for his guidance. This research would not have been complete without his help and direction. Moreover, I thank the Industrial and system engineering department, especially Marilyn Houck, and Jennifer Barretta for their help and support.

I thank all my lab mates Shaunak, Chaitanya, Pritam, Akul and Anuvhav for making the work enjoyable. It was a wonderful experience working in the Brinkman Lab and AMPrint Center. I thank everyone who made this possible.

Finally, I would like to thank my parents Sangita and Jalandhar Sahoo for their constant support, love and blessings. My special thanks to Sourav Das and Pritam Poddar for their support and motivation.

There are only so many people I can name here, but I thank everyone who made my study at RIT exciting and memorable.

Table of Contents

Table of Figures

List of Tables

1. Introduction

Additive manufacturing, commonly known as 3D printing or rapid prototyping, has historically been used to create prototypes directly from 3D CAD models. As prototype quality has improved over time, printed models have been directly used as the final product [1]. Thus, in 2009, the ASTM F42 Committee officially adopted "Additive Manufacturing" (AM) as the appropriate name for processes used to produce functional parts [2]. A 3D Computer-Aided-Design (CAD) model is sliced into numerous layers in this process. Each slice layer is fed to a 3D printer that successively prints one layer on top of another, forming the complete part. Fused Deposition Modeling (FDM), Stereolithography (SLA), Selective Laser Sintering (SLS), and Material Jetting are some of the common AM process. These processes offer a large selection of materials that include plastics, polymers, ceramics, metals and even biological tissue [1]. The ability to produce complex geometries without expensive tooling is a rather attractive feature of AM, and its use is warranted when there is a requirement for extensive customization.

Printed electronics are electronic devices that are fabricated by printing conductive materials (e.g. inks, pastes, conductive thermoplastics) onto substrates such as papers and polymers. The traditional electronics fabrication process involves multiple sequential steps and use of plating and etching chemicals that are typically absent in printed electronics processes. Hence, in recent years there has been a significant rise in the use of printed electronics. Cost analysis suggests that printed electronics have lower cost per unit area but higher cost per function than conventional electronics fabrication processes [3]. This is largely due to lower resolution of printed electronics processes.

When combined, AM and printed electronics techniques can be used to simultaneously manufacture mechanical and electronic features within the same part. This can lead to faster delivery of prototypes and functional parts as well as reduced assembly time [4][5]. In this work, AM and printed electronics have been combined to explore embedded electronics.

1.1 Embedded Electronics

Recent developments in printed electronics have enabled researchers to pursue a new field of research called embedded electronics [6]. Embedded electronics allow the integration of mechanical and electrical components in a single device to perform a specific task. Electronic watches, coffee makers, and alarm devices are all based on embedded electronics. Improvements in processes such as Aerosol Jet printing and micro extrusion have made it possible to print very fine conductive lines even on curved surfaces. This approach can replace conventional circuit boards by integrating the electronics directly on the parts [7]. An example of this approach is taken by Voxel8 which has developed a platform for printing embedded electronics [8].

1.2. Statement of Need

A major cause of equipment failure is due to wires and interconnects failing at the joints due to weak solder or loose interconnects. If we can connect those components using printed conductive traces embedded inside the casing, we can eliminate these wires and joints to reduce the rate of equipment failure and to reduce assembly labor costs.

To demonstrate this, a case study was done on a DeWALT DCD985M2 20V Hammerdrill. The inside of the drill is shown in Figure 1. As can be seen, there are

multiple wire harnesses, connectors and joints. By redesigning the drill and printing all the conductive traces to connect the components, the number of potential points of failure can be reduced [9].

While there are examples of 3D printed electronics in the literature, a primary aim of this research is to do an exploratory study of how component geometry and printing parameters affect electrical conductivity using recently developed materials.

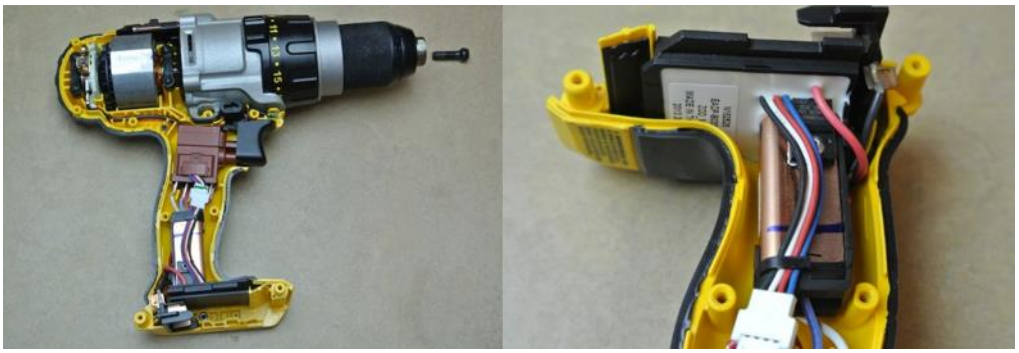

Figure 1: Internal structure of DEWALT drill [9]

2. Literature Review

To be able to print functional embedded electronics parts, we need a clear understanding of the available inks and printing process. This literature review is focused on exploring the various processes and inks suitable for our application.

2.1 Conductive Inks

Conductive inks can include both organic and metallic components. In general, conductive inks are available as solutions, colloids or in suspensions. Even direct printing of low melting point metals has been done [10]. The rheology of the inks depends upon the application and the printing process used.

2.1.1 Organic Inks

Conductive inks require a low resistance path over which electrons can flow when a potential difference is applied. The polymer based inks rely on the conductivity along the long polymer backbone and between polymer chains. In case of conductive particles dispersed in a non-conductive matrix, the conductivity depends on the direct contact between conductive particles [11].

In a composite system where a conductive material is bound together by a non-conductive matrix, it is necessary to have inter-particle connectivity. There exists a point called the percolation threshold at which the volume fraction of the conductive phase is high enough that a continuous pathway for electron travel exists, and electronic conductivity starts to increase rapidly [11].

PEDOT:PPS and graphene are two commercially available materials which can be formulated in inkjet printable forms. Various high quality prints have been obtained using water soluble single layered graphene oxide (GO) and few layered graphene oxide (FGO) [12]. Thin film transistors (TFT) have been successfully fabricated using PEDOT-PPS with a combination of spin coating and inkjet printing [13].

Polymer inks usually have relatively low electrical conductivity compared with the metallic inks. Some polymer inks require curing in an inert atmosphere to reduce oxidation.

2.1.2 Metallic Inks

Metallic inks are preferred over polymer inks for certain applications as they typically provide better electrical conductivity. Metal inks are typically of two types: metal nanoparticle inks (NP) and metal organic decomposition inks (MOD).

The nano particle inks are suspensions of nanoparticles typically in either water or organic solvents. The solvent easily evaporates leaving the nanoparticles behind. The high surface area to volume ratio of the nanoparticles enables sintering at low temperature. However, these inks are very prone to agglomeration of the suspended particles which can lead to clogging of nozzles [14].

The organometallic inks, or MOD's, have the advantage of not being in the form of particulate suspensions. This lessens the risk of agglomeration and nozzle clogging. Higher conductivities have been achieved using MOD inks compared to NP inks. MODs are also often cured at lower temperatures than those of NP inks [14].

At present, some of the most conductive inks are formulated with silver nanoparticles. This is because Ag possesses the highest electrical conductivity among metals and is resistant to oxidation. Gold is another such metal, but the high cost of Au ink makes it less desirable for commercial use. Ag can be replaced by less expensive conductive metals such as copper or aluminum, but the real challenge lies in avoiding their oxidation during thermal curing [15]. Recent advances in NP research have enabled inkjet printing of Cu NP inks with decreased oxidation and higher conductivity [16].

2.2. Printing Methods

2.2.1 Flexography

Flexography is a widely used process in the packaging and printing industry. It works on the kiss impression method using flexible plate and anilox technology. It can be used to print on a wide variety of substrates, thus making it a very popular choice in the printing industry. The printing unit consists of an inking unit, a plate cylinder and an impression cylinder. The inking unit generally uses an anilox with either a doctor blade or a fountain roller. An anilox cylinder is a chrome or ceramic cylinder with tiny grooves etched onto it. These grooves control the cell volume of the anilox. Anilox of different cell volumes are used according to the required ink film thickness. The doctor blade together with the fountain roller control the ink metering (i.e. the amount of ink on the anilox cylinder). The ink on the anilox roller is transferred to the printing plate fixed on the plate cylinder. It is from the plate cylinder that the ink gets printed on the substrate pressed to it by the impression cylinder. The impression roller controls the pressure between the printing plate and the substrate. A typical pressure of 0.3 Mpa is used for printing. The ink used can have a dynamic viscosity of 50-500 Mpa.S. An ink film thickness of 0.8 to 2.5 µm

can be obtained by this method. A schematic diagram of the flexography process is shown below in Figure 2 [17].

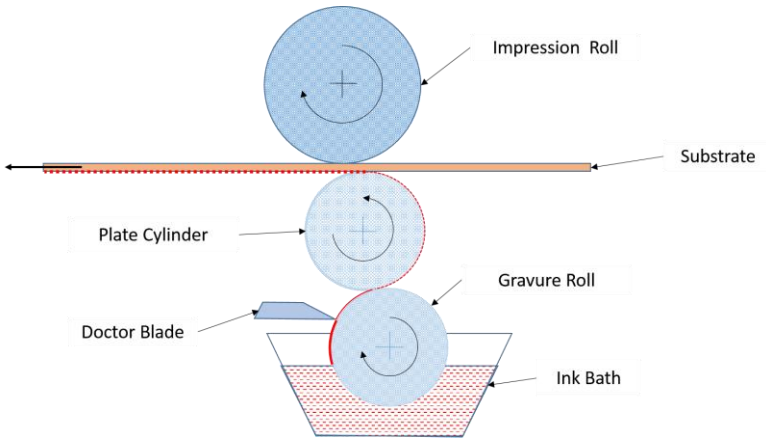

Figure 2: Flexography process (adapted from [17])

2.2.2 Gravure Printing

Gravure printing is an established low cost printing method for various printed electronics applications. The major advantage of gravure printing is its high resolution and ability to print low viscosity inks. Moreover, gravure printing can deposit high ink thickness on the substrate, which is a major limitation of flexography printing.

The gravure printing setup is much simpler than flexography. It basically consists of four units: the ink fountain, the carrier or gravure cylinder, the doctor blade and the impression cylinder. The core element of this process is the engraved cylinder, which carries the image design to be printed. The substrate is passed between the impression roller and engraved cylinder dipped in the ink fountain. The doctor blade scrapes excess

ink off of the engraved cylinder [18]. A schematic diagram of the gravure printing process is shown in Figure 3.

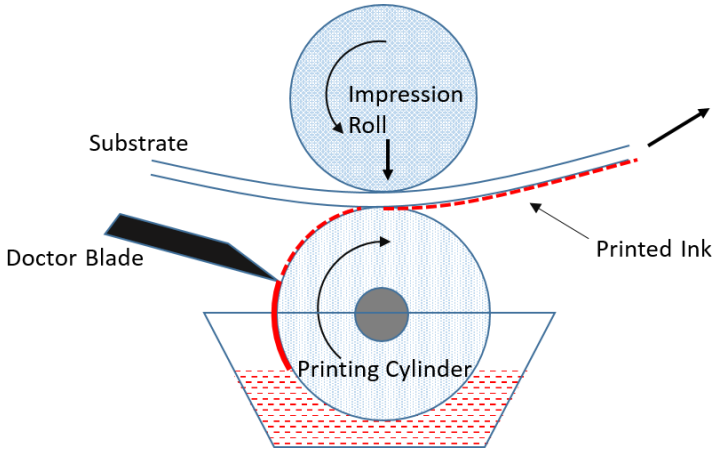

Figure 3: Gravure printing (adapted from [18])

2.2.3 Screen Printing

Screen printing is one of the earliest printing technique dating back to 960 AD [19]. In this process, a viscous ink is pushed through a screen mesh with a squeegee. A polymer emulsion is used to block the negative of the image on the screen mesh. This ensures selective passage of the ink through the screen. Despite the advantages of low cost and simple operation of screen printing compared to other printing processes, the resolution is typically limited to approximately 100 µm at printing speeds up to 30 m/min [17]. Figure 4 shows the working of a screen printing process.

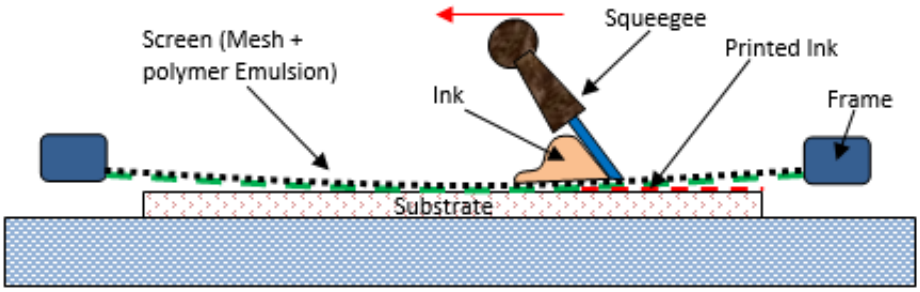

Figure 4: Screen printing (adapted from [17])

2.2.4 Inkjet Printing

Since its foundation in the nineteenth century, inkjet printing has become one of the most widely used printing technologies. In recent years, this technology has become very a popular research interest for functional printing. The first inkjet process developed was continuous inkjet (CIJ). In CIJ printing, the droplet deposition location is controlled by the variation of an electrostatic field applied to the stream of drops being ejected from the nozzle. The unused drops are collected and recirculated. This process is not always suitable for printing functional materials, as recirculation of ink may degrade the property of the inkjet inks [14].

The more commonly used technique for functional materials is drop-on-demand (DOD) inkjet printing. In DOD print heads, a controlled electrical pulse signal ejects ink out of the nozzle. These print heads can be classified as either the thermal or piezoelectric type.

In a thermal type inkjet head, current is passed through a resistive heater placed near the nozzle. The heater quickly heats a small volume of ink up to its bubble nucleation temperature. Thermal expansion forces ink out of the nozzle thus forming a droplet. As

the heater switches off, the bubble collapses and the ink is refilled by capillary action. Due to the heating of inks, this process finds limited application with thermally sensitive inks [14] [13]. Figure 5 shows a thermal inkjet head.

In piezo-electric print heads, a small piezo-electric element is placed inside the ink chamber as shown in Figure 6. When a voltage is applied, the piezoelectric element expands and forces a drop of ink through the nozzle. The relaxation of the piezo actuator draws new ink into the channel. The amount and rate of ink ejected can be controlled by varying the magnitude and frequency of the electrical pulses. This makes piezoelectric inkjet printing very useful for printing functional materials. The main disadvantage of the inkjet process is the low viscosity range of the usable ink – typically 5 – 20 Mpa-S [14] [13] [17].

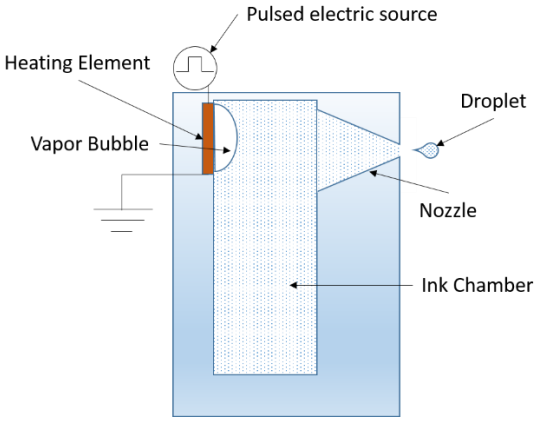

Figure 5: Thermal inkjet head

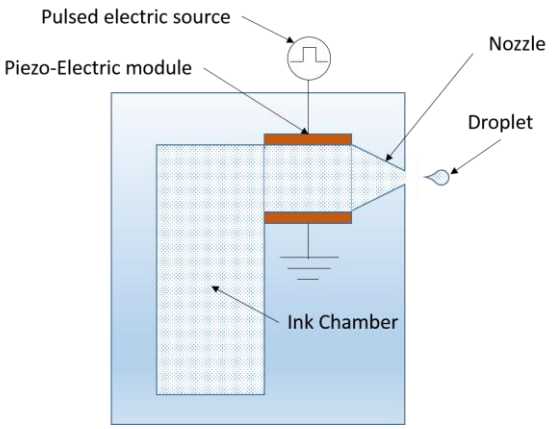

Figure 6: Piezo-electric inkjet head

2.2.5 Micro- Extrusion

Micro-extrusion is an example of Direct-Write (DW) technology. DW processes can print two or three dimensional functional structures directly on substrates without any tooling or masks [20]. In general, liquid inks such as colloidal inks or nanoparticle suspensions are deposited on the surface of the substrate which forms the basis for the desired structure. After deposition, the ink is solidified by evaporation or thermal curing [1].

The main parts of a micro-extrusion system are the nozzle, motion control sub-system, and pump or plunger. The size of the nozzle determines the size and shape of the deposit. It also affects the range of ink viscosity and particle size that can be printed. The motion control system determines the dimensional accuracy, speed and maximum size of the print. The pump controls how accurately the process can be started or stopped. It also determines the speed of the print. The pump system can be pneumatically controlled or motor assisted. Figure 7 shows a motor assisted micro-extrusion system.

Under the right conditions, micro-dispensing systems are able to print inks having viscosities from 1- 1000000 cP. Recent research has demonstrated printing of ceramic composite inks using a motor assisted micro-syringe (MAM) [21].

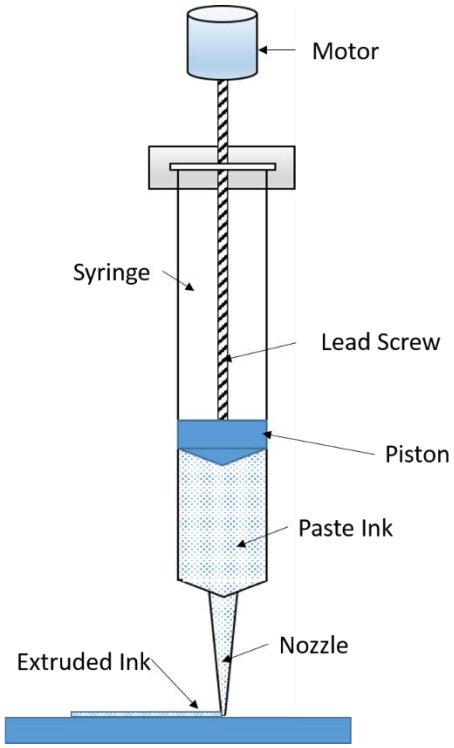

Figure 7: Micro-extrusion System

2.2.6 Aerosol Jet Printing

Aerosol Jet printing (AJP) is a non-contact DW process that can print low viscosity inks and colloidal suspensions on both flat and non-planar surfaces. The working principle of this process relies upon aerodynamic focusing. The basic AJ system consists of an atomizing module and a focusing module as shown in Figure 8 [22].

The atomizing module forms the aerosol mist using an ultrasonic or pneumatic atomizer. Ultrasonic atomizers are used for inks with low viscosities (typically <20 cP) and particle sizes (typically <100 nm). Pneumatic atomizers are used for high viscosity inks (typically

up to 1000 cP) and particle sizes (typically up to 500 nm) [23]. The aerosol mist is then delivered to the deposition head where a co-axial sheath gas aerodynamically focuses the mist on the substrate. The print head is capable of focusing the mist up to 1/10th of the nozzle diameter [24].

The movement of the AJ head is controlled by a computer program according to the code. The AJ mist is continuous, so a programmed shutter is used to collect the excess material when it is not printing. Since AJP is a non-contact printing process, it can be used to print traces that conform to non-planar surfaces while maintaining a stand-of distance of ~5mm [24].

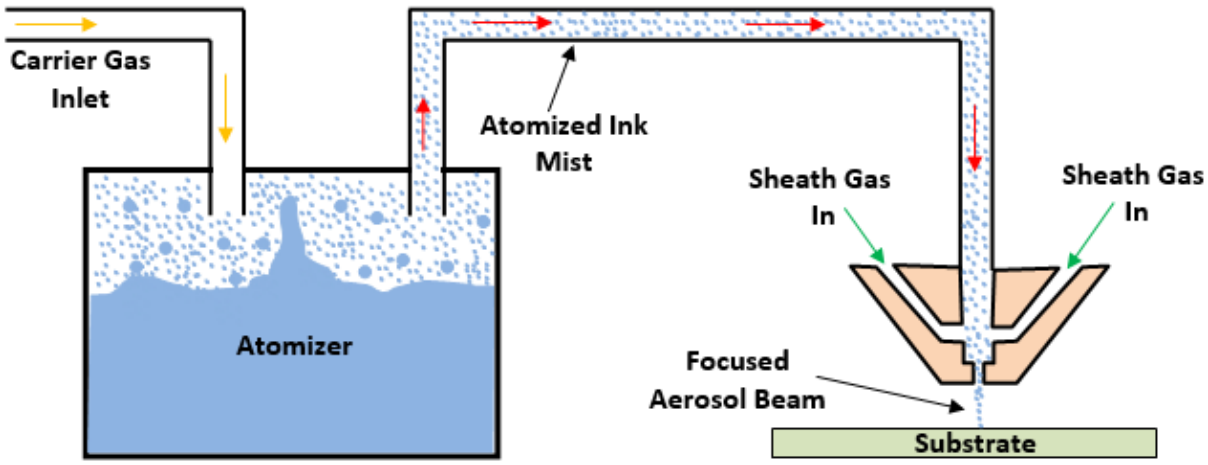

Figure 8: Aerosol jet system

2.2.7 Fused Deposition Modeling (FDM)

This technology was first developed for rapid prototyping in the early 1990s. Since then, research and development has made it a viable alternative for the manufacture of finished parts. FDM is also known by various other names such as Fused Filament Fabrication

(FFF) and Melt Extrusion Manufacturing (MEM). The basic principle behind all these process remains the same [25].

The core elements of the FDM system are the filament feeding system, the liquefying zone, the nozzle and the build-platform. The feeding mechanism is generally a filament feed supplied via a pinch roller system controlled by an electric stepper motor. The most commonly used filaments are Acrylonitrile Butadine Styrene (ABS) and Polylactic Acid (PLA). The filament is then passed through a liquefying zone, which is basically a resistively heated chamber. The filament is heated to a temperature above its glass transition temperature (T_g) at which point the filament softens enough to be extruded. For ABS the T_g is around 105 °C. This melt of liquid plastic is pushed through the nozzle by the solid filament entering the liquefying chamber. On leaving the nozzle, the extruded material is deposited on the print bed where it solidifies. After the layer is printed, the print bed moves down or the nozzle moves up to facilitate printing of the next layer [25] [1]. A schematic diagram showing the working of FDM is shown in Figure 9.

Parts produced by the FDM process are anisotropic and have greater strength in the direction of the deposition plane (X-Y) versus the layer direction (z-axis). The dimensional accuracy and resolution of the printed parts depends upon the process and product design parameters and the type of filament used. Recent research shows process parameter can be controlled to print parts with targeted physical properties [26].

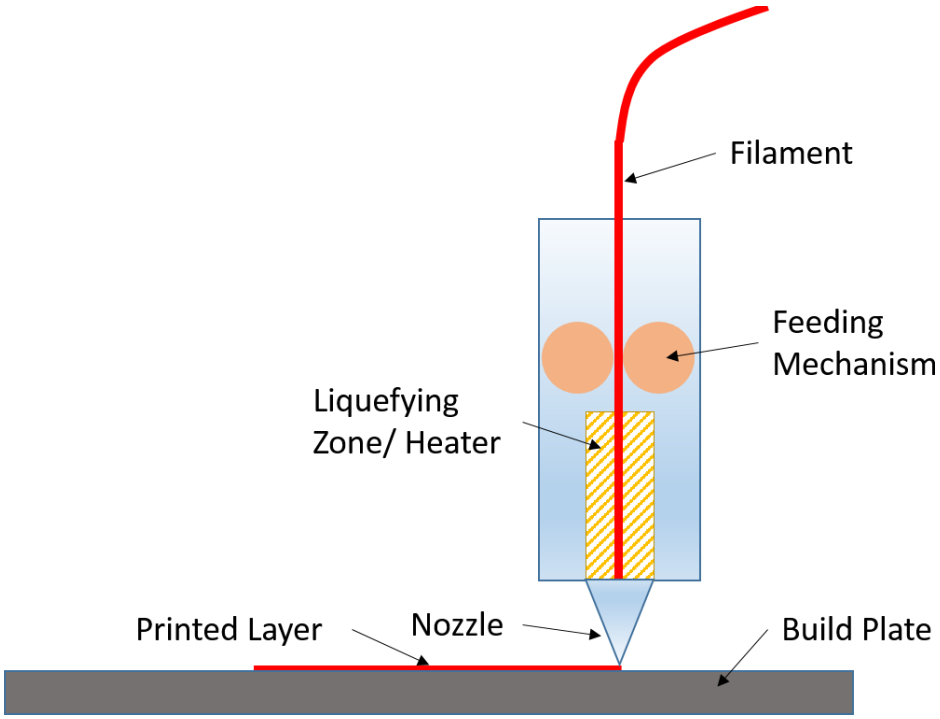

Figure 9: Fused deposition modeling system

2.3. Curing Techniques

2.3.1 Thermal Curing

Thermal curing is one of the oldest sintering processes used to cure inks. Heating the inks to a specific temperature releases the solvent enabling the particles to come together and form continuous links. Typical sintering temperatures for conductive inks range widely from approximately 100 °C to 300 °C depending on particle size distribution. During curing, the organic solvents evaporate leaving behind nanoparticles and possibly some organic adhesion promoters. Since this process requires heating of inks, substrates with lower melting points such as Polyethylene Terephthalate (PET) cannot be used at higher curing temperatures [27]. At lower curing temperatures, the increase in resistivity of the conductive traces is observed due to incomplete removal of solvents and other organic components. Research suggests that a gradual increase of curing temperature gives the

highest conductivity [28]. Recent developments in ink formulation show that it is possible to cure some silver inks at room temperature [29]. This has made the use of temperature sensitive substrates such as paper and PET possible.

2.3.2 Microwave Sintering

Conductive patterns of silver, gold and copper have shown good results with microwave sintering. The curing time can be considerably reduced to 240 sec with minimal heating of the substrate. This enables the use of temperature sensitive substrate materials. The major limitation of the process is the penetration depth of about 1.3 to 1.6 μm. This limits the thickness of the conductive traces that can be cured. Moreover, substrate that react to microwaves cannot be used in this process [30].

2.3.4 Photonic Curing

Photonic curing is a process of sintering nanoparticle based inks using high intensity, short bursts of broad spectrum light from xenon gas filled lamps. Since the curing time is very short (typically on the order of milliseconds), the high thermal mass of solid substrate materials allows substrates to be processed with minimal heating. This enables the use of paper and other temperature sensitive substrate materials. Low curing times also make high speed roll-to-roll (R2R) printing and curing possible. Electrical conductivity on the order of 4x bulk resistivity has been obtained for silver inks using this process at room temperature [31], [32].

2.4 3D Printed Electronics

With the advancement of additive manufacturing technology, researchers have been developing technologies to fabricate embedded components for end use products.

Researchers have successfully demonstrated procedures to print parts with embedded electronic components using Stereolithography (SLA) and direct printing of conductive traces [33]. Using the same technology, researchers have demonstrated a printed prototype of a temperature sensor with embedded components [34] and an electrical relay [35]. Others have demonstrated a 3D printed motor rotor using ultrasonic welding to embed copper wire directly into the thermoplastic [36].

2.5 Research Objectives

The objective of this literature review was to describe available methods for printing conductive traces embedded inside a functional part. Researchers have demonstrated procedures to print functional parts using SLA and ultrasonic welding. These processes have led to very impressive results, however, they are fairly complex and the necessary equipment is quite expensive. The emphasis of this research is to evaluate options for simple low cost processes to print conductive traces. There are several printing options for doing this. Analog printing processes such as flexography, gravure and screen printing are best suited for printing on planar substrates. However, they are not suitable for digital 3D printing due to their use of fixed patterns such as engraved cylinders or screen patterns. Aerosol Jet and inkjet printing processes are digital; however, they are considerably more expensive and complex than simple material extrusion processes (e.g. FDM or microextrusion). The FDM and microextrusion processes have the same basic working principle (i.e extruding highly viscous material through a nozzle). The deposition tools can be mounted on a single motion control system which allows for uninterrupted printing and material changes. The focus of this research is to study very

low cost options for multi-material 3D printing with embedded electrically conductive traces. Thus the decision was made to focus on material extrusion techniques.

A wide variety of materials are available for extrusion processes. PLA was selected for the FFE process due to its availability and low cost. Silver nanoparticle ink was chosen for the micro-extrusion process as it is easily cured, it has good electrical properties and it is widely used for printed electronics.

3. Methods and Materials

The main objectives of this thesis are to (1) demonstrate simple and low-cost processes to print conductive traces embedded inside a functional part, (2) evaluate the electrical performance of the printed conductive materials; and (3) use experimental results to make recommendations on how to design parts for maximum performance. For demonstrating this process, a basic flashlight consisting of a light emitting diode (LED) and a battery was printed. The FFE process was used to print the structure of the flashlight. For the conductive trace, micro extrusion with a motor assisted syringe extruder was used.

3.1. Conductive Silver Ink

3.1.1 Selection of Materials

Polylactic Acid (PLA) was used to print the flashlight housing. PLA was chosen over other thermoplastic materials since it is durable and has good end use properties. PLA is a plant based thermoplastic, it has low environmental impact, and it can be recycled [37] [38].

For conductive traces, silver nanoparticle ink from DUPONT (PE872) was used. PE872 is a nanoparticle silver ink with a nominal sheet resistivity < 100 mΩ/sq/25µm. It is best suited for low voltage application (<3V DC), and its ability to be printed on stretchable surfaces makes it an excellent choice [39].

Figure 10: Silver nano-particle ink from DuPONT

3.1.2 Equipment

A HYREL 3D System 30 printer was used to print the samples. The System 30 can accommodate up to four independent print heads. The MK-1 print head was used to print PLA, and a modified EMO-25 paste extruder was used to print silver ink.

3.1.2.1 MK-1 Print Head

The MK-1 print head is a thermoplastic filament extruder built by Hyrel 3D. It is equipped with a 0.5 mm diameter nozzle and a stepper motor for feeding the 1.75 mm diameter thermoplastic filament. To print very fine structures, the nozzle size was changed to 0.4 mm diameter. Figure 11 shows a photo of the original MK-1 extruder provided by Hyrel 3D.

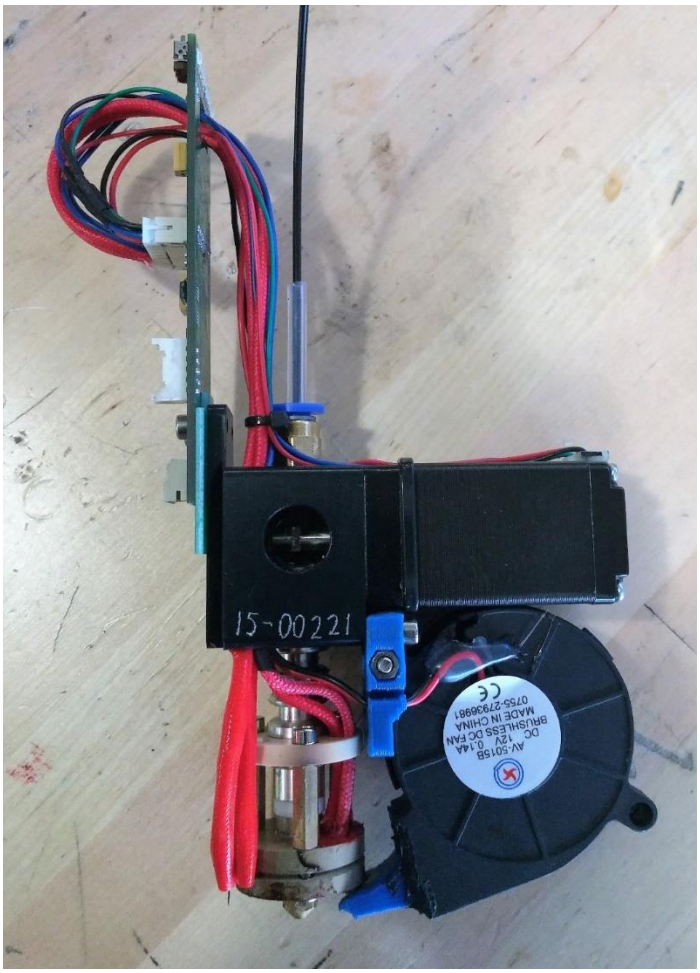

Figure 11: Mk-1 extruder from Hyrel 3D

3.1.2.2 EMO-25

The EMO-25 is a syringe type paste extruder, driven by a stepper controller coupled with a gear box. Originally, the system was developed to print Plasticine. For this research, the tool was modified to work with a 5cc disposable dispensing syringe to print inks and pastes. Figure 12 shows the EMO-25 extruder before and after modification.

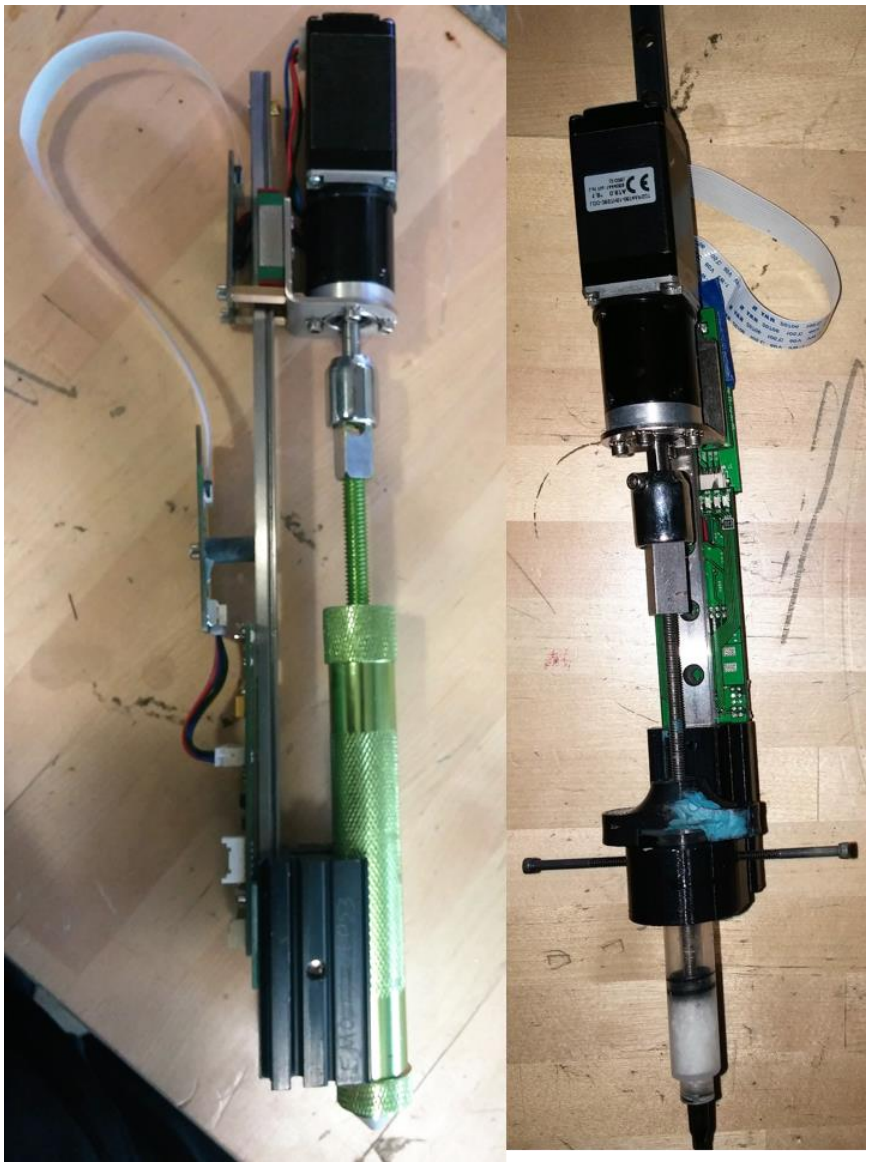

Figure 12: EMO-250 extruder before and after modification

3.1.3 Fabrication Methodology

The following work procedure has been used to print the LED flashlight.

1. A model of the flashlight was designed in Solidworks 2014. This model contains both the fixtures for holding the components and the conductive traces connecting them.
2. Conductive traces and the base part were saved into individual STL files.
3. Using the slic3r slicing software, the base stl was first sliced with a printing speed of 30 mm/sec and saved into a file named *base.gcode*.
4. The base part with the conductive traces was then sliced with a printing speed of 5 mm/sec and saved into a file named *ink.gcode*. This was done for the different printing requirements of PLA and silver ink.
5. A software package called Repetier was used to modify the *base.gcode* file to include the portion of conductive ink from the *ink.gcode* file.
6. After compiling both gcode files into one, the merged file was imported into Repetrel (the control software for Hyrel 3D) and printed.
7. After printing the part with the conductive ink, it was placed in an electric oven at 110 $^{\circ}$C for 30-50 mins and then tested for conductivity. If the printed silver ink was not sufficiently conductive following insertion of the battery and LED, then it was set in the oven for another 30 mins.

3.1.4 Experimentation Results

Initial prints that were filled with silver ink did not cure even after keeping them in the oven for several hours. This may have occurred because of the following reasons:

- The temperature was not sufficient for curing.
- Solvent was not able to escape due to insufficient venting in the 3D printed structure.

To check the effect of temperature, the oven temperature was increased to 130 $^{\circ}$C, and the part was kept there for 30 mins. Though the silver ink was cured, significant warping was observed in the part shown in Figure 13.

Figure 13: Warping of part at 130 $^{\circ}$C

Since the first solution did not work out, a new approach was used to let the vapors escape. A large cavity with an air gap of 2mm was designed with the intent of better allowing solvents to dry and vapors to escape, and silver ink was printed within this enlarged gap shown in Figure 14 . The redesigned part was placed in an oven for the ink to cure in 30-40 mins. The silver ink cured and became electrically conductive as confirmed by the glowing LED. This redesign suggests that an air gap may have an impact on the curing effectiveness of this silver ink. Figure 15 shows the final part printed and cured with the air gap.

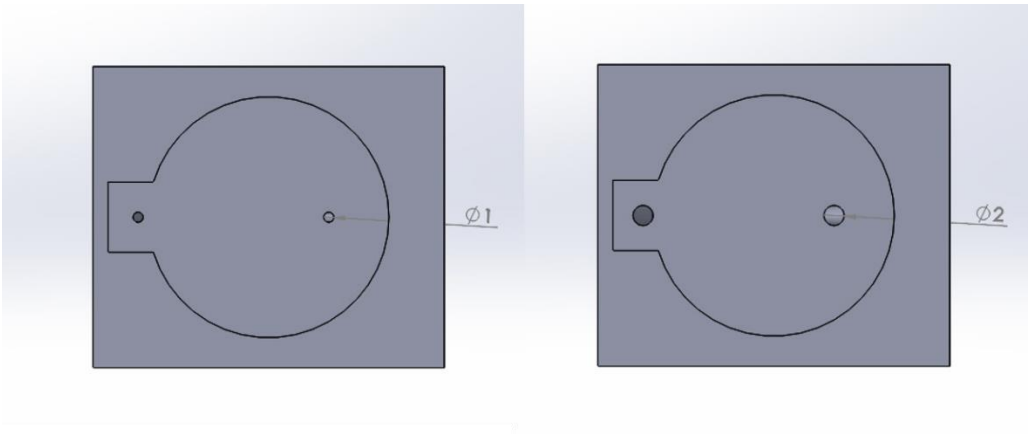

Figure 14: Ink cavity redesigned to 2mm for better curing

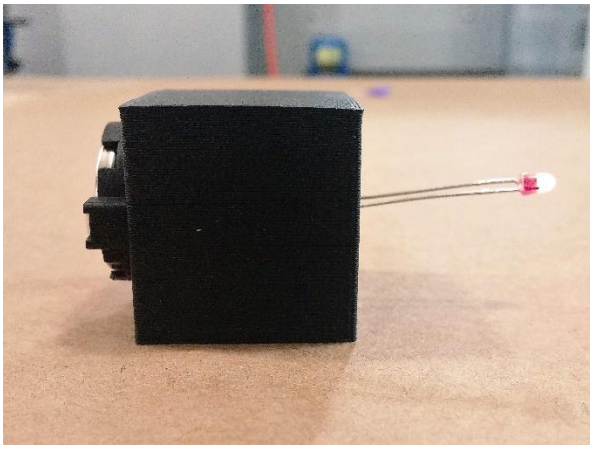

Figure 15: Final printed assembly

An alternative solution to the curing challenge is to cure the ink just after is has been printed. To do this, the ink was cured using a hot air gun for 3 mins. It should be noted that transfer of the semi-completed print to an oven and then subsequent transfer of the part back to the Hyrel 3D printer for completion of the print would be problematic. The hot air gun was simply used for a quick test of the idea in an admittedly uncontrolled manner. As we can see in Figure 16, warping on the top surface of the part was observed. Although this approach should not be ruled out based on an uncontrolled temperature

experiment, in-situ drying and curing of the conductive silver ink would require considerably more effort than the aforementioned thermal post-cure approach.

Figure 16: Warping of top surface when heated with hot air gun

3.2 Conductive Graphene PLA

A second approach to printing of conductive materials was assessed using thermoplastic PLA filled with electrically conductive graphene. This required a determination of the printing parameters and other factors that affect the conductivity of printed samples.

3.2.1 Equipment and Materials

For this experiment, a Hyrel 3D System 30 printer was used with the MK-1 printed head having a nozzle diameter of 0.5 mm. All printing was done with Black Magic 3D graphene PLA filament developed by Graphene Labs.

Recommended printing parameter for the filament as suggested by the manufacturer are as follows:[40]

- Extruder temperature: 220°C
- Platform temperature: 50°C
- Print speed: 1800 mm/min
- Nozzle size: >0.5 mm
- Extrusion multiplier: 1.1

Figure 17: Black magic 3D graphene filament

3.2.2 Proposed Methodology

To check the feasibility of the process and find appropriate printing parameters, an experiment was designed with the following factors:

1. Print Length (mm)
2. Part Orientation Relative To Print Direction (degrees)
3. Aspect Ratio
4. Temperature (°C)
5. Layer Height (mm)

The response variable for the experiment was electrical resistance measured between the opposing surfaces (i.e. green faces in Fig. 18) at orientations of 0°, 55°, and 90° as shown in Figure 18. The resistance was measured using a Fluke multimeter with the probe plates pressed to the measuring surface. The measuring surface was coated with Dupont 5021 silver nanoparticle paste and was cured in an oven for 5 minutes shown in Figure 21. This was done to improve the surface contact for the measurement of resistance.

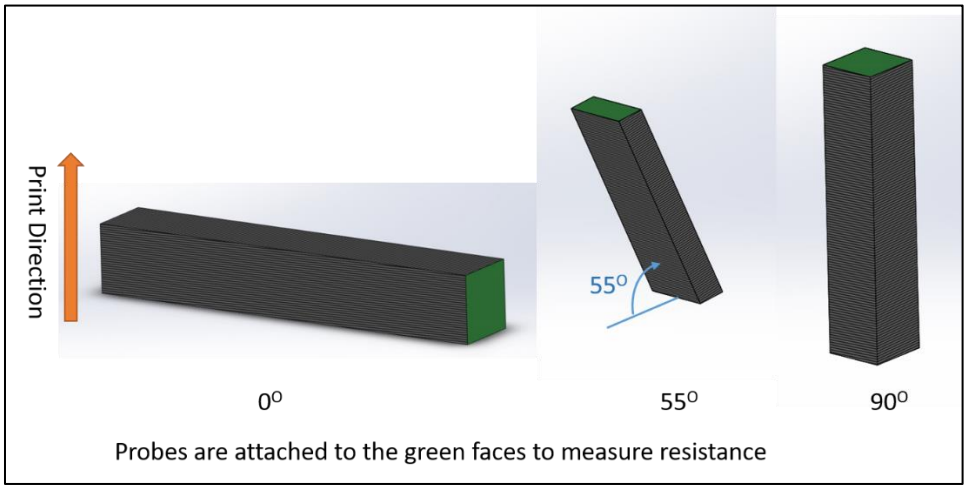

Figure 18: Direction of measurement for each orientation

Figure 19: Fluke multimeter

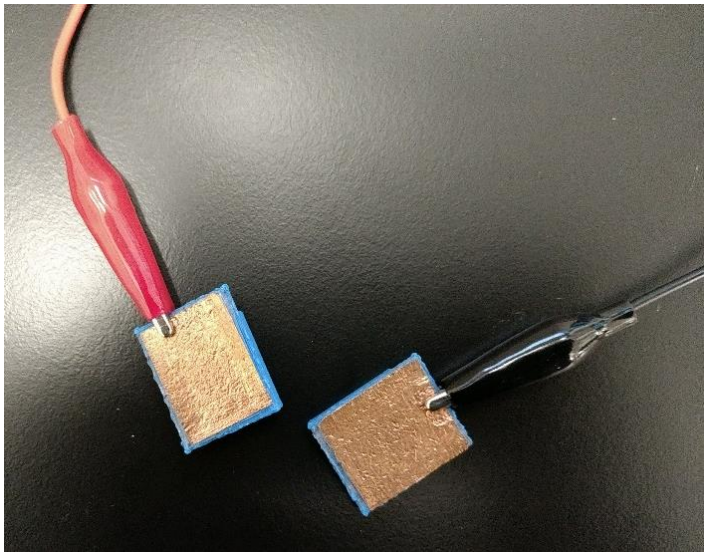

Figure 20: Probe plates to measure resistance

Figure 21: Measuring surface coated with Dupont 5021 silver paste

Length- Length of the printed material through which electricity travels affects the amount of resistance offered to the flow of the electrons. Theoretically, the resistance should increase as the conductive path length increases. In this research, conductive path lengths of 20 mm, 30 mm and 50 mm were used.

Orientation- The prints were assessed with respect to electrical conductivity relative to the print orientation. In other words, it was desired to determine whether conductivity across a given length parallel to the print direction differed from conductivity across the same length perpendicular to the print direction, and if so, by how much. This result is helpful for deciding upon the best printing orientation of the conductive filaments when designing composite parts. For this research, orientations of 0°, 55°, and 90° relative to the horizontal axis were used. A representation of this is shown in Figure 18.

Aspect Ratio- This is defined as the ratio of a part's height to its width. For this research, each aspect ratio test sample had the same X-axis length. When viewed along the X-axis, the aspect ratio was defined as the ratio of the cross sectional height in the Z-axis to the cross sectional width in the Y-axis. The aspect ratio levels used in this research were 1:4, 1:1 and 4:1 (i.e. 4 mm x 16 mm, 8 mm x 8 mm and 16 mm x 4 mm respectively). Figure 22 shows the cross-section of parts at the 0° orientation.

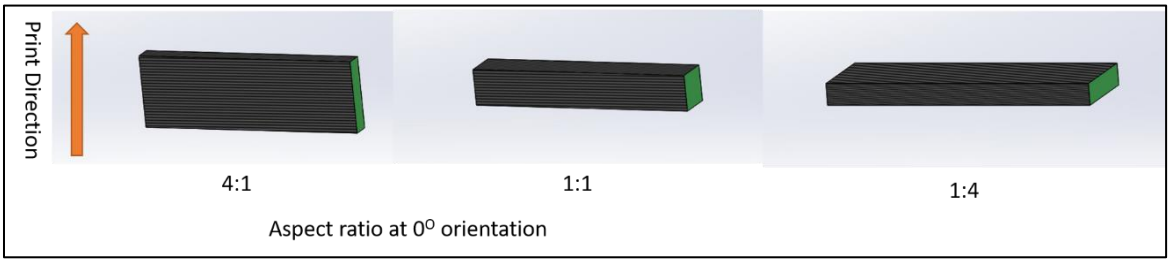

Figure 22: Aspect ratios of printed parts at 0^{o} orientation

Nozzle Temperature: Temperature affects the bonding quality and density between the layers, which in turn affects the conductive path for electrons to flow. The levels used for this research were 220 °C, 200 °C, and 190 °C.

Layer Height: Layer height determines the thickness of the deposited beads and the contact area of each layer. A narrow bead requires more traces to print a given width of area and therefore produces more interfaces between printed traces that electrons must pass through. For this research, layer thicknesses of 0.2, 0.3 and 0.4 mm were chosen.

Table 1: Factors and levels for the experiment

Factors	**Levels**		
Length	20 mm	30 mm	50 mm
Orientation	0°	55°	90°
Aspect ratio	1:4	1:1	4:1
Temperature	190°C	200°C	220°C
Layer height	0.2 mm	0.3 mm	0.4 mm

Temperature and layer height affect the bonding quality the between layers, whereas length, orientation and aspect ratio affect the basic structure of the print thereby having a greater effect on the resistance. A screening experiment was therefore conducted to find the optimum value for these factors while other factors were kept constant (i.e. length = 20 mm, orientation 0°, and aspect ratio = 1:1). A full factorial design of experiments with 5 replicates was conducted. The design for the screening experiment is given in Appendix A.

Analysis of Variance

Source	DF	Adj SS	Adj MS	F-Value	P-Value
Regression	4	67.72	16.9292	0.33	0.854
Temperature	1	6.34	6.3362	0.12	0.727
Layerheight	1	0.47	0.4713	0.01	0.924
Layerheight*Layerheight	1	36.82	36.8167	0.72	0.403
Temperature*Layerheight	1	4.05	4.0500	0.08	0.780
Error	25	1273.75	50.9500		
Lack-of-Fit	1	12.15	12.1500	0.23	0.635
Pure Error	24	1261.60	52.5667		
Total	29	1341.47			

Figure 23: Analysis of variance for screening experiment

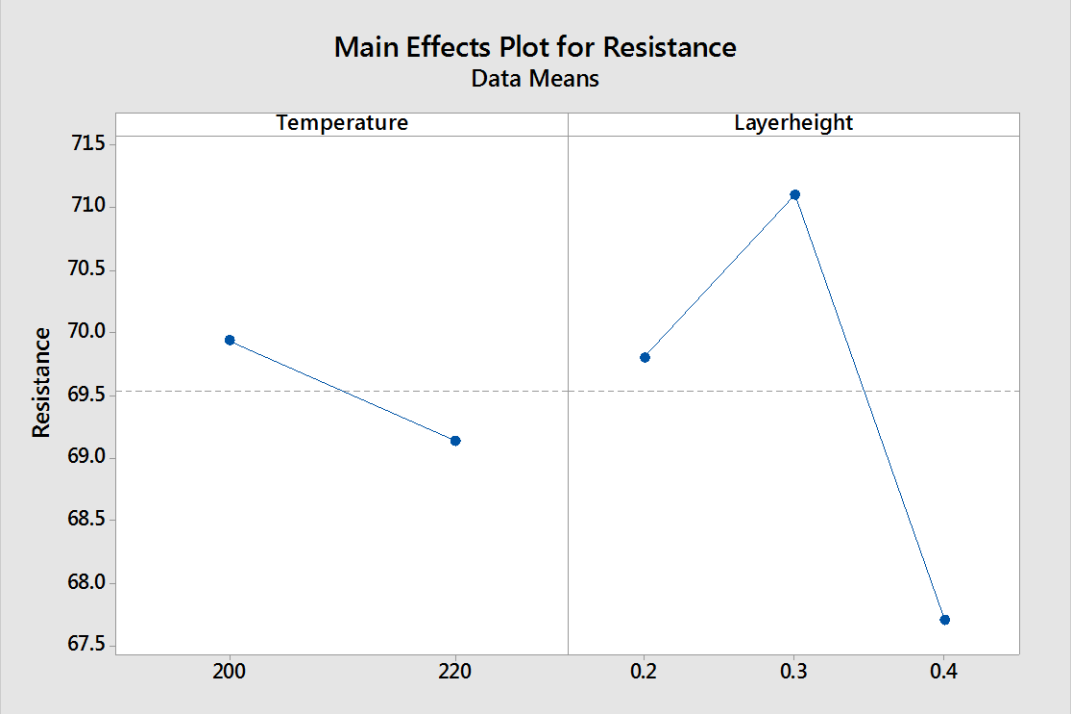

Figure 24: Main effect plot for screening experiment

As seen in Figure 23, the temperature and layer height had high P-values implying a statistically minimal effect on electrical resistance within the testing range. From the main effect graph in Figure 24, we see that the resistance only changes from 70Ω to 69Ω as temperature goes from 200^{o}C to 220^{o}C which confirms our hypothesis that temperature has a relatively small effect on electrical resistance. Similarly from the main effect plot for layer height, we see an initial increase and then a decrease in the resistance. However, the overall resistance range from 71 Ω to 67.75 Ω is still small. For the final experiment, the temperature and layer height were therefore fixed at 220 °C and 0.4 mm respectively.

With just three major factors to consider (length, orientation and aspect ratio) a full factorial experiment with 6 replicates and blocking on the replicates was designed. Blocking on the replication was done to batch print the experiment, where each block

was printed in a single day. This reduced the effect of uncontrolled factors such as ambient temperature, humidity etc. on the experiment. To normalize the effect of size on the experiment, resistivity was used rather than resistance using the equation below. The design for the final experiment is given in Appendix B.

$$Resistivity(\rho) = \frac{Resistance(\Omega) * Area(mm \text{ x } mm)}{Length(mm)}$$

3.2.3 Experimental Results

As seen from the results in Figure 25, the Orientation and Aspect Ratio factors all have P-values less than a confidence interval of α=0.1. This means that these factors are statistically significant, or they have a significant effect on the resistance of the printed graphene PLA. The orientation*orientation term is also significant suggesting the relation between resistivity and orientation is not linear.

Analyzing the residuals in Figure 26 to check for compliance with the DOE assumptions, we find that the residuals are normally distributed, have equal variance, and are independent.

Regression Analysis: resistivity versus Length, Orientation, Aspect ratio

Method

Categorical predictor coding (-1, 0, +1)

Continuous predictor standardization
Levels coded to -1 and +1

Predictor	Low	High
Length	20	50
Orientation	0	90

Analysis of Variance

Source	DF	Adj SS	Adj MS	F-Value	P-Value
Regression	11	126271	11479.2	23.61	0.000
Length	1	1835	1835.0	3.77	0.054
Orientation	1	83022	83021.9	170.74	0.000
Aspect ratio	2	5459	2729.5	5.61	0.004
Length*Length	1	87	87.2	0.18	0.673
Orientation*Orientation	1	11515	11515.3	23.68	0.000
Length*Orientation	1	72	72.0	0.15	0.701
Length*Aspect ratio	2	1479	739.7	1.52	0.222
Orientation*Aspect ratio	2	10095	5047.7	10.38	0.000
Error	150	72936	486.2		
Lack-of-Fit	15	9257	617.1	1.31	0.205
Pure Error	135	63679	471.7		
Total	161	199207			

Model Summary

S	R-sq	R-sq(adj)	R-sq(pred)
22.0508	63.39%	60.70%	57.99%

Figure 25: Regression analysis of the resistance

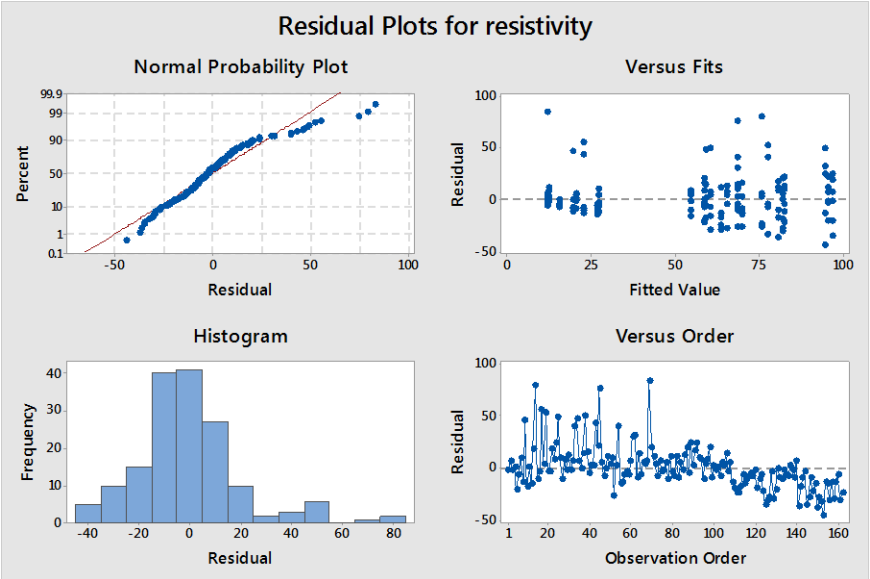

Figure 26: Residual plot for final experiment

3.2.4 Discussion of Results

The main effects plot of resistivity in Ω-mm as a function of length, orientation, and aspect ratio is shown in Figure 27. The interpretation of results for each experimental factor are explored in detail in the following sections.

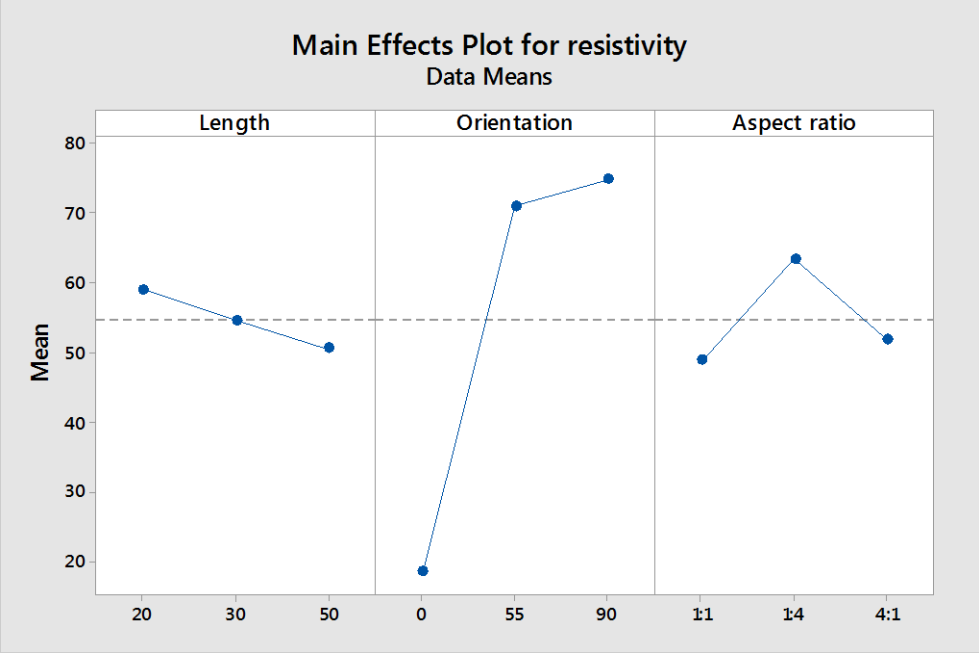

Figure 27: Main effect plot for length, orientation and aspect ratio

Length:

Basic principles suggest that a material's resistivity should remain constant irrespective of its size. From the main effects plot shown in Figure 27, we can see that the slope of the fitted curve for resistivity decreases linearly from ~59 Ω-mm to 50 Ω-mm as the length increases from 20mm to 50mm. This strongly suggests that the 3D printed material does not behave as a homogenous bulk material and is instead affected by the printing parameters. Figure 29 offers a potential explanation for this behavior. In Figure 29(a), the top-down view of toolpaths for the 20mm, 30mm, and 50mm long samples are shown.

The resistance of each printed sample is measured end-to-end. On the left and right ends of each sample, there are 8 traces printed perpendicular to the path that electrons flow when traveling end-to-end through the samples. Consequently, electrons must traverse 16 interfaces (8 per side) between printed material traces. It is hypothesized that these interfaces have relatively poor conductivity. Although the 20mm, 30mm, and 50mm long samples each have exactly the same number of these interfaces, the conductive path through those interfaces is a smaller percentage of the overall path length as the sample length increases. This would potentially explain the progressive decrease in resistivity as sample length increases.

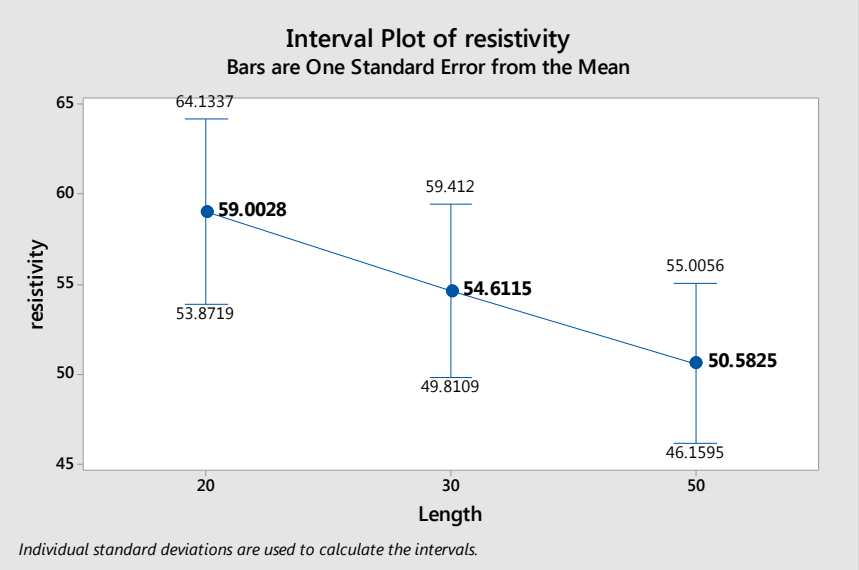

Figure 28: Standard error for length

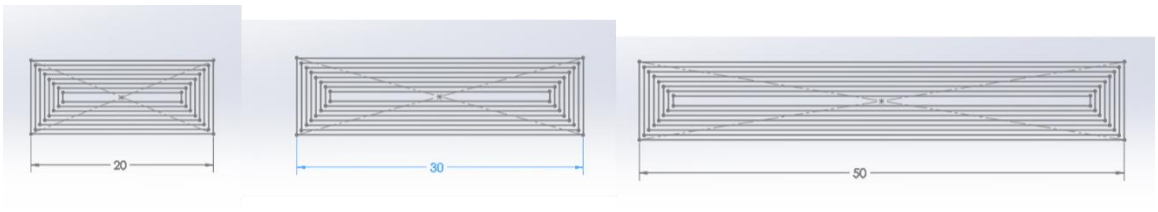

(a)

(b)

Figure 29: (a) Top view of printed toolpaths for 20mm, 30mm, and 50mm samples; (b) Close-up view of toolpath on one end of sample

Orientation:

Orientation appears to be the most significant factor that affects the resistivity as shown in Figure 30. The lowest resistivity is observed at an orientation of 0 degrees. Referring back to the orientation convention shown in Figure 18, an orientation of 0 degrees represents the condition where the printed filament rows are oriented parallel to the direction of electron flow. This results in very low interfacial resistance between printed traces other than those associated with the contour printing shown in Figure 29. At the 55 degree and vertical 90 degree print orientations, the resistivity increases drastically because of the large number of interfacial boundaries between layers (22 interfacial layers at 0 degrees, 116 interfacial layers at 55 degrees, and 142 interfacial layers at 90 degrees). At the junction of each layer, there is increased resistance to free flow of electrons resulting in higher resistivity. Figure 31 shows a micrograph of layer transitions.

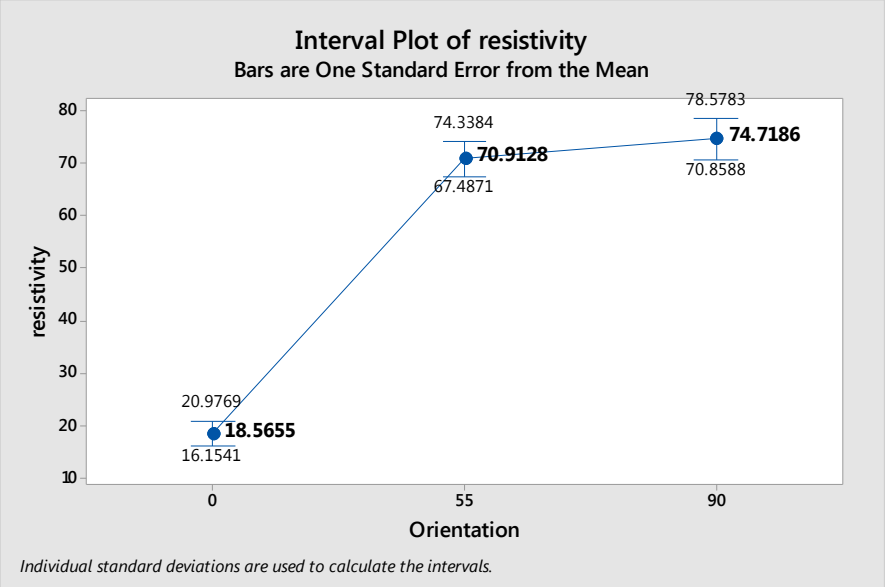

Figure 30: Standard error for orientation

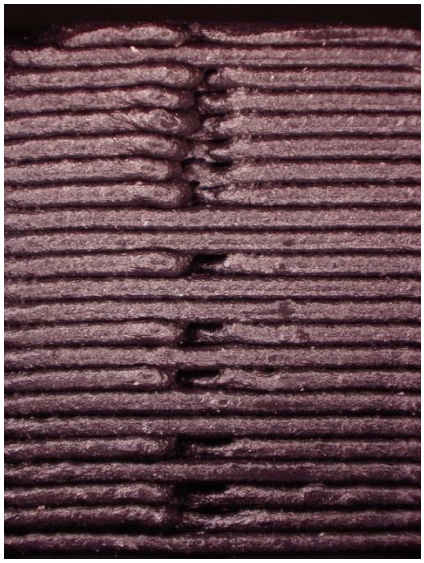

Figure 31: Micrograph showing layer transition

Aspect ratio:

In a homogenous bulk material, resistivity should be unaffected by the aspect ratio. However, this is not the case with the 3D printed samples. Referring to the aspect ratio convention in Figure 22, Figure 32 shows resistivity as a function of aspect ratio. The difference in resistivity can again be explained by the image in Figure 33 which shows

that the number of interfacial transitions through which electrons flow is markedly different between the 4:1 and 1:4 samples. It is therefore not surprising that the 1:4 sample has to lowest resistivity. Resistivity of the 1:1 sample is counterintuitive though. The number of interfacial transitions for the 1:1 sample is between that of the 1:4 and 4:1 samples, hence one would expect the sample resistivity to be between those two extremes. This will require greater study.

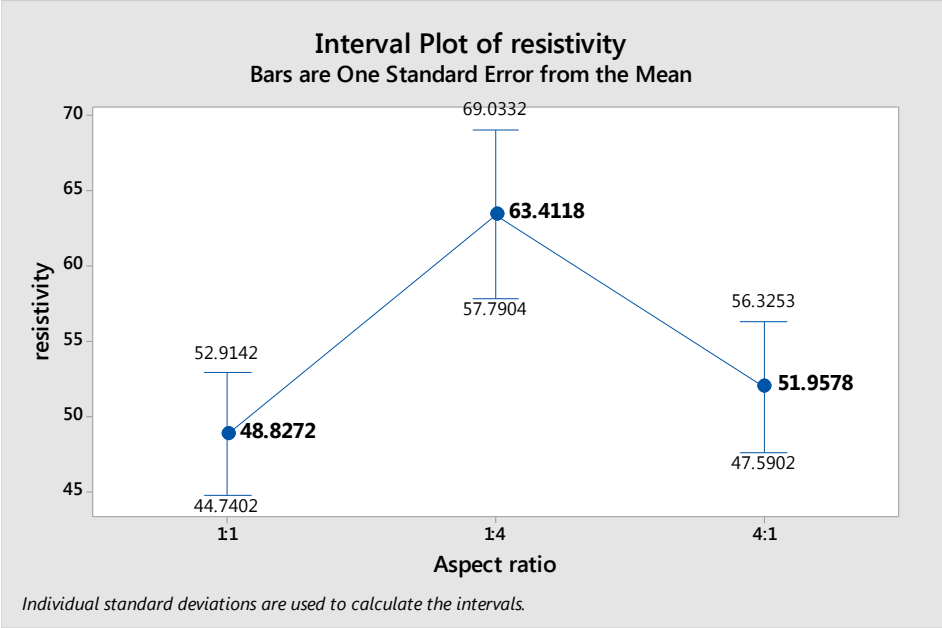

Figure 32: Standard error for aspect ratio

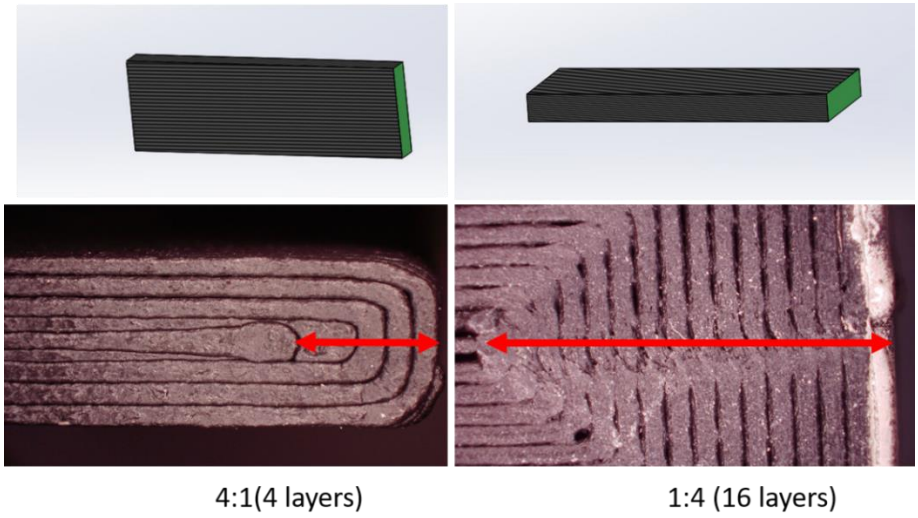

Figure 33: Comparison between 4:1 and 1:4 aspect ratio

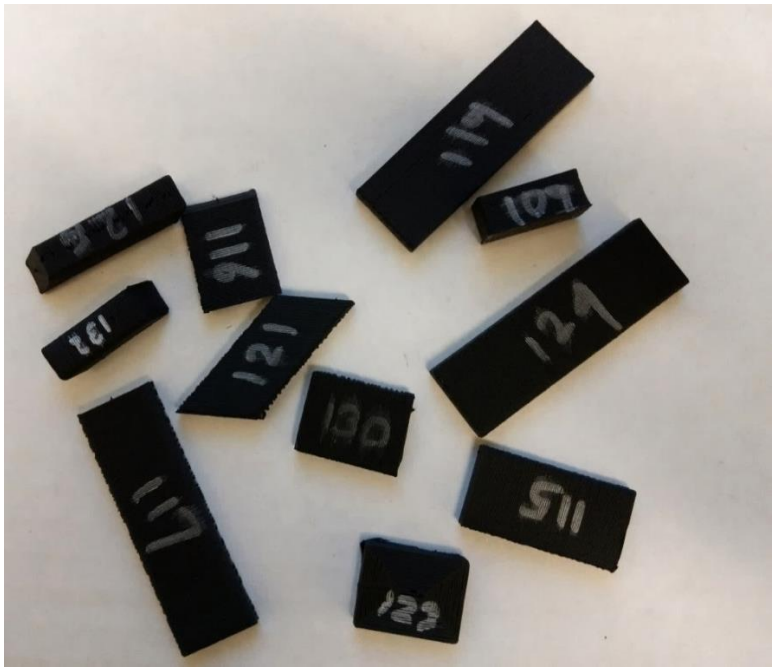

Figure 34: Printed sample from final experiment

4.2.4 Issues with Graphene PLA

The graphene PLA was found to be a difficult material to print. The most common issues observed were:

- Clogging of nozzles.
- Oozing during extrusion moves.

The graphene particles tended to stick to the rough interior of the brass nozzle, thereby clogging the nozzle. Graphene is also a good conductor of heat, hence it transmits heat quickly up to the unmelted filament above the hot-end. Keeping material heated in the nozzle for prolonged time can cause melting or softening of filament at the pinch feed rollers, resulting in failure to extrude material. It is therefore recommended to print at the lowest possible temperatures and higher speeds with the shortest possible non-printing times in order to minimize these issues. Another challenge is retention of moisture. The

PLA is hygroscopic in nature, which means it absorbs moisture from the environment [41]. When the filament is heated, the steam formed from this moisture tries to escape through the nozzle potentially resulting in poor print quality. To avoid this, the filament is to be stored in a dry place and pre-heated to 50 °C for 3 hours to remove all moisture.

5. Conclusions and Future Research Directions

This exploratory study has considered two different processing routes for embedding printed electronics within a 3D printed part. In the first approach, conductive silver paste is extruded and then dried/cured following completion of the part. In the second approach, an electrically conductive thermoplastic filament is extruded rather than silver paste.

Both of these processes and materials have separate uses. The silver ink is highly conductive and very expensive, while the graphene PLA has considerably lower conductivity but is relatively inexpensive. Therefore, the silver ink is more suitable for printing conductive traces requiring higher conductivity and/or when the part is less price sensitive.

As for the graphene PLA filament, the printing process is quite simple. The relatively low electrical conductivity limits its applications though. The graphene PLA filament can be used as a resistor in the printed circuit or in places where a voltage drop is needed as in the case of a flash light. From the results of the designed experiment, we can conclude that the length, orientation and aspect ratio need to be considered when designing the printed circuit. The graphene PLA gives lowest resistance when:

1. Overall print conductive path length is minimized
2. The number of interfacial printed trace boundaries to be traversed is minimized in either the horizontal or vertical directions.

The initial experiments with the silver nanoparticle ink and the graphene PLA revealed the shortcomings in the process and the limitations of the materials. Overcoming these shortcomings will make the process and material more feasible to use for printed electronics.

The printing process for the silver nanoparticle ink can be modified to include a curing mechanism using low power laser or infrared heat source to enable printing and curing of ink at the same time. Another possible change would be to develop an ink that can be cured more easily.

The graphene PLA filaments have a tendency to block the nozzle. This problem can be minimized using higher diameter nozzle or a smoother nozzle like a ceramic or stainless-steel nozzle. The graphene percentage in the PLA filament can be increases to check if the resistance can be lowered enough to be used for practical application. Moreover, the uses of metal infused filaments might improve the performance of printed circuits.

Lastly, it is strongly recommended that a more complete study in which the 3D printer in-fill pattern and trace stepover distance are modified be conducted. In this research, offset contour in-fill patterns were used. Other infill strategies that minimize the number of interfacial trace boundaries should be explored. Likewise, optimization of the printed trace stepover distance to increase density of the printed structures is also suggested.

References

[1] I. Gibson, D. W. Rosen, and B. Stucker, *Additive Manufacturing Technologies*. 2009.

[2] "Committee F42 on Additive Manufacturing Technologies." [Online]. Available: http://www.astm.org/COMMITTEE/F42.htm. [Accessed: 04-Aug-2015].

[3] V. Subramanian *et al.*, "Printed electronics for low-cost electronic systems: Technology status and application development," *Solid-State Device Res. Conf. 2008. ESSDERC 2008. 38th Eur.*, vol. 34, pp. 17–24, 2008.

[4] E. Atzeni and A. Salmi, "Economics of additive manufacturing for end-usable metal parts," *Int. J. Adv. Manuf. Technol.*, vol. 62, no. 9–12, pp. 1147–1155, Oct. 2012.

[5] S. H. Huang, P. Liu, A. Mokasdar, and L. Hou, "Additive manufacturing and its societal impact: a literature review," *Int. J. Adv. Manuf. Technol.*, vol. 67, no. 5–8, pp. 1191–1203, Jul. 2013.

[6] C. M. Shemelya *et al.*, "3D printing multi-functionality: Embedded RF antennas and components," *Antennas and Propagation (EuCAP), 2015 9th European Conference on*. pp. 1–5, 2015.

[7] D. Espalin, D. W. Muse, E. MacDonald, and R. B. Wicker, "3D Printing multifunctionality: structures with electronics," *Int. J. Adv. Manuf. Technol.*, vol. 72, no. 5–8, pp. 963–978, Mar. 2014.

[8] "Voxel8: 3D Electronics Printing." [Online]. Available: http://www.voxel8.co/. [Accessed: 24-Dec-2015].

[9] "DeWALT DCD985M2 20V Hammerdrill/Driver – A look inside | Tools In Action - Power Tools and Gear." [Online]. Available: http://professional-power-tool-guide.com/2013/09/dewalt-dcd985m2-20v-hammerdrilldriver-a-look-inside/. [Accessed: 23-Dec-2015].

[10] Q. Liu and M. Orme, "High precision solder droplet printing technology and the state-of-the-art," *J. Mater. Process. Technol.*, vol. 115, no. 3, pp. 271–283, 2001.

[11] D. R. Gamota, P. Brazis, K. Kalyanasundaram, and J. Zhang, *Printed organic and molecular electronics*. Springer Science & Business Media, 2013.

[12] L. Huang, Y. Huang, J. Liang, X. Wan, and Y. Chen, "Graphene-based conducting inks for direct inkjet printing of flexible conductive patterns and their applications in electric circuits and chemical sensors," *Nano Res.*, vol. 4, no. 7, pp. 675–684, 2011.

[13] B. J. de Gans, P. C. Duineveld, and U. S. Schubert, "Inkjet Printing of Polymers:

State of the Art and Future Developments," *Adv. Mater.*, vol. 16, no. 3, pp. 203–213, 2004.

[14] G. Cummins and M. P. Y. Desmulliez, "Inkjet printing of conductive materials: a reviewnull," *Circuit World*, vol. 38, no. 4, pp. 193–213, Nov. 2012.

[15] A. Kamyshny, J. Steinke, and S. Magdassi, "Metal-based inkjet inks for printed electronics," *Open Appl. Phys. J.*, vol. 4, pp. 19–36, 2011.

[16] B. K. Park, D. Kim, S. Jeong, J. Moon, and J. S. Kim, "Direct writing of copper conductive patterns by ink-jet printing," *Thin Solid Films*, vol. 515, no. 19, pp. 7706–7711, Jul. 2007.

[17] H. Kipphan, *Handbook of Print Media: Technologies and Production Methods*. Springer Science & Business Media, 2001.

[18] E. Hrehorova *et al.*, "Gravure Printing of Conductive Inks on Glass Substrates for Applications in Printed Electronics," *Display Technology, Journal of*, vol. 7, no. 6. pp. 318–324, 2011.

[19] A. Sheng, "Why Ancient Silk Is Still Gold: Issues in Chinese Textile History," *Ars Orient.*, vol. 29, pp. 147–168.

[20] J. Bruneaux, D. Therriault, and M.-C. Heuzey, "Micro-extrusion of organic inks for direct-write assembly," *J. Micromechanics Microengineering*, vol. 18, no. 11, p. 115020, Nov. 2008.

[21] W. Huang, X. Zhang, Q. Wu, and B. Wu, "Fabrication of HA/ β - TCP scaffolds based on micro- syringe extrusion system," *Rapid Prototyp. J.*, vol. 19, no. 5, pp. 319–326, Jul. 2013.

[22] B. H. King and M. J. Renn, "Aerosol Jet® Direct Write Printing for Mil-Aero Electronic Applications," *WHITEPAPER - Optomec*, 2008.

[23] C. Goth, S. Putzo, and J. Franke, "Aerosol Jet printing on rapid prototyping materials for fine pitch electronic applications," *Proc. - Electron. Components Technol. Conf.*, pp. 1211–1216, 2011.

[24] T. Blumenthal, V. Fratello, G. Nino, K. Ritala, Q. Integrated, and P. S. Suite, "Conformal printing of sensors on 3D and flexible surfaces using Aerosol Jet deposition," vol. 8691, pp. 1–9, 2013.

[25] B. N. Turner and S. A. Gold, "A review of melt extrusion additive manufacturing processes: II. Materials, dimensional accuracy, and surface roughness," *Rapid Prototyp. J.*, vol. 21, no. 3, pp. 250–261, Apr. 2015.

[26] D. Roberson, C. M. Shemelya, E. MacDonald, and R. Wicker, "Expanding the applicability of FDM-type technologies through materials development," *Rapid*

Prototyp. J., vol. 21, no. 2, pp. 137–143, Mar. 2015.

[27] E. Halonen, T. Viiru, K. Östman, A. L. Cabezas, and M. Mantysalo, "Oven sintering process optimization for inkjet-printed Ag Nanoparticle ink," *IEEE Trans. Components, Packag. Manuf. Technol.*, vol. 3, no. 2, pp. 350–356, 2013.

[28] J. R. Greer and R. A. Street, "Thermal cure effects on electrical performance of nanoparticle silver inks," *Acta Mater.*, vol. 55, no. 18, pp. 6345–6349, Oct. 2007.

[29] S. Magdassi, M. Grouchko, O. Berezin, and A. Kamyshny, "Triggering the Sintering of Silver Nanoparticles at Room Temperature," *ACS Nano*, vol. 4, no. 4, pp. 1943–1948, Apr. 2010.

[30] J. Perelaer, B.-J. de Gans, and U. S. Schubert, "Ink-jet Printing and Microwave Sintering of Conductive Silver Tracks," *Adv. Mater.*, vol. 18, no. 16, pp. 2101–2104, 2006.

[31] J. West, M. Carter, S. Smith, J. Sears, and S. R. City, "Photonic Curing of Silver Nanoparticle Based Inks," *NSTI-Nanotech*, vol. 2, pp. 210–213, 2010.

[32] K. a Schroder, S. C. Mccool, W. F. Furlan, and K. Lane, "Broadcast Photonic Curing of Metallic Nanoparticle Films," *NSTI-Nanotech*, vol. 3, no. 512, pp. 198–201, 2006.

[33] A. J. Lopes, E. Macdonald, R. B. Wicker, and W. M. Keck, "Integrating stereolithography and direct print technologies for 3D structural electronics fabrication."

[34] A. Lopes, M. Navarrete, F. Medina, J. Palmer, E. Macdonald, and R. Wicker, "EXPANDING RAPID PROTOTYPING FOR ELECTRONIC SYSTEMS INTEGRATION OF ARBITRARY FORM."

[35] J. A. Palmer *et al.*, "Stereolithography: A basis for integrated meso manufacturing." University of Texas at Austin (freeform), 01-Jan-2005.

[36] E. Aguilera *et al.*, "3D Printing of Electro Mechanical Systems."

[37] B. M. Tymrak, M. Kreiger, and J. M. Pearce, "Mechanical properties of components fabricated with open-source 3-D printers under realistic environmental conditions," 2014.

[38] M. Kreiger *et al.*, "Environmental Impacts of Distributed Manufacturing from 3-D Printing of Polymer Components and Products," *MRS Proc.*, vol. 1492, no. 3–4, p. mrsf12-1492-g01-02, Jan. 2013.

[39] "PRODUCT DESCRIPTION."

[40] "Conductive Graphene 3D Printing PLA Filament." [Online]. Available:

http://www.blackmagic3d.com/Conductive-p/grphn-175.htm.

[41] M. P. Arrieta, J. López, A. Hernández, and E. Rayón, "Ternary PLA–PHB–Limonene blends intended for biodegradable food packaging applications," *Eur. Polym. J.*, vol. 50, pp. 255–270, 2014.

Appendix

Appendix A

Design table for screening experiment

StdOrder	RunOrder	PtType	Blocks	Temperature ^{0}C	Layerheight mm	Resistance Ω
26	1	1	5	200	0.3	60
25	2	1	5	200	0.2	75
29	3	1	5	220	0.3	70
28	4	1	5	220	0.2	70
30	5	1	5	220	0.4	65
27	6	1	5	200	0.4	60
4	7	1	1	220	0.2	65
3	8	1	1	200	0.4	60
2	9	1	1	200	0.3	76
1	10	1	1	200	0.2	68
6	11	1	1	220	0.4	55
5	12	1	1	220	0.3	69
8	13	1	2	200	0.3	79
11	14	1	2	220	0.3	69
10	15	1	2	220	0.2	70
7	16	1	2	200	0.2	70
9	17	1	2	200	0.4	75
12	18	1	2	220	0.4	80
14	19	1	3	200	0.3	62
15	20	1	3	200	0.4	71
17	21	1	3	220	0.3	71
13	22	1	3	200	0.2	60
16	23	1	3	220	0.2	70
18	24	1	3	220	0.4	75
21	25	1	4	200	0.4	70
20	26	1	4	200	0.3	85
19	27	1	4	200	0.2	78
24	28	1	4	220	0.4	66

Appendix B

Design table for final experiment.

RunOrder	Blocks	Length **mm**	Orientation **Degrees**	Aspect ratio	Resistance **Ω**	Resistivity **Ω.mm**
1	3	50	0	1:4	10.8	13.37
2	3	20	90	1:1	24.0	71.13
3	3	30	0	1:4	4.6	9.47
4	3	50	55	1:1	50.0	59.87
5	3	20	55	1:4	20.0	61.57
6	3	50	55	1:4	62.0	76.33
7	3	20	0	1:4	7.2	22.17
8	3	20	0	1:1	4.1	12.88
9	3	50	0	1:1	52.0	65.17
10	3	30	55	1:1	22.0	44.88
11	3	50	0	4:1	9.2	11.95
12	3	30	90	4:1	27.0	53.81
13	3	20	90	1:4	38.0	114.06
14	3	20	55	4:1	48.0	154.61
15	3	30	55	1:4	34.0	68.97
16	3	50	90	1:4	77.0	91.25
17	3	30	0	1:1	38.0	77.44
18	3	30	0	4:1	11.0	24.23
19	3	20	90	4:1	43.0	129.42
20	3	50	55	4:1	45.0	54.43
21	3	50	90	1:1	43.0	51.42
22	3	50	90	4:1	64.0	77.06
23	3	20	55	1:1	22.0	76.68
24	3	30	90	1:4	59.0	117.72
25	3	30	90	1:1	56.0	108.29
26	3	20	0	4:1	11.0	36.18
27	3	30	55	4:1	28.0	57.13
28	4	50	55	4:1	55.0	66.52
29	4	50	0	1:1	14.0	17.54
30	4	20	90	1:1	26.0	77.06
31	4	20	55	1:4	26.0	80.04
32	4	50	90	1:1	51.0	60.99
33	4	30	55	4:1	53.0	108.13
34	4	50	55	1:1	88.0	105.38
35	4	20	0	1:4	6.3	19.40

36	4	30	0	1:4	5.0	10.29
37	4	30	90	4:1	42.0	83.71
38	4	30	90	1:4	72.0	143.66
39	4	50	90	4:1	61.0	73.45
40	4	50	0	1:4	8.2	10.15
41	4	20	0	4:1	9.0	29.60
42	4	50	0	4:1	10.4	13.51
43	4	30	0	1:1	32.0	65.21
44	4	50	90	1:4	98.0	116.13
45	4	20	55	1:1	41.0	142.90
46	4	20	90	1:4	34.0	102.05
47	4	20	0	1:1	6.0	18.85
48	4	30	0	4:1	9.0	19.83
49	4	30	55	1:4	45.0	91.28
50	4	30	90	1:1	33.0	63.81
51	4	50	55	1:4	74.0	91.10
52	4	30	55	1:1	18.0	36.72
53	4	20	55	4:1	24.0	77.30
54	4	20	90	4:1	39.0	117.38
55	1	30	55	1:1	24.0	48.96
56	1	30	90	4:1	28.0	55.81
57	1	20	0	4:1	6.0	19.73
58	1	20	90	1:4	31.0	93.05
59	1	50	0	1:4	7.0	8.67
60	1	20	90	1:1	24.0	71.13
61	1	20	55	1:1	28.0	97.59
62	1	30	90	1:4	63.0	125.70
63	1	30	0	1:1	6.6	13.45
64	1	50	55	1:1	61.0	73.05
65	1	20	0	1:1	6.5	20.42
66	1	50	0	4:1	12.6	16.36
67	1	30	0	4:1	10.6	23.35
68	1	30	55	1:4	43.0	87.22
69	1	30	0	1:4	46.0	94.70
70	1	20	55	1:4	33.0	101.59
71	1	50	55	1:4	76.0	93.57
72	1	50	90	1:1	48.0	57.40
73	1	30	90	1:1	27.0	52.21
74	1	50	55	4:1	54.0	65.31
75	1	50	90	1:4	78.0	92.43
76	1	50	90	4:1	47.0	56.59
77	1	20	55	4:1	25.0	80.52
78	1	50	0	1:1	7.3	9.15
79	1	30	55	4:1	39.0	79.57
80	1	20	0	1:4	3.0	9.24

81	1	20	90	4:1	23.0	69.22
82	6	50	90	1:4	89.0	105.47
83	6	30	0	1:1	6.2	12.63
84	6	30	90	1:1	34.0	65.75
85	6	30	0	1:4	4.5	9.26
86	6	20	55	1:1	23.0	80.16
87	6	50	55	1:4	83.0	102.19
88	6	20	90	4:1	24.0	72.23
89	6	30	90	1:4	59.0	117.72
90	6	30	90	4:1	36.0	71.75
91	6	30	55	1:4	48.0	97.37
92	6	20	90	1:4	40.0	120.06
93	6	30	55	1:1	36.0	73.44
94	6	50	90	1:1	52.0	62.19
95	6	20	0	1:1	5.0	15.71
96	6	20	90	1:1	23.0	68.17
97	6	50	90	4:1	55.0	66.22
98	6	50	55	4:1	64.0	77.41
99	6	50	0	1:1	8.2	10.28
100	6	20	0	1:4	4.5	13.86
101	6	30	0	4:1	8.1	17.84
102	6	50	55	1:1	50.0	59.87
103	6	50	0	1:4	6.3	7.80
104	6	20	55	4:1	25.0	80.52
105	6	50	0	4:1	11.0	14.28
106	6	30	55	4:1	40.0	81.61
107	6	20	0	4:1	7.0	23.02
108	6	20	55	1:4	28.0	86.20
109	2	20	0	1:1	3.8	11.94
110	2	50	55	1:1	33.0	39.52
111	2	20	55	4:1	16.0	51.54
112	2	50	55	1:4	48.0	59.10
113	2	30	90	1:1	22.0	42.54
114	2	50	55	4:1	43.0	52.01
115	2	30	90	1:4	40.0	79.81
116	2	50	0	1:1	7.5	9.40
117	2	50	90	4:1	42.0	50.57
118	2	30	55	4:1	31.0	63.25
119	2	50	0	1:4	6.1	7.55
120	2	20	0	1:4	3.1	9.55
121	2	30	55	1:4	30.0	60.85
122	2	50	90	1:1	36.0	43.05
123	2	20	0	4:1	6.0	19.73
124	2	50	90	1:4	62.0	73.47
125	2	20	90	4:1	14.0	42.14

126	2	30	55	1:1	16.0	32.64
127	2	30	90	4:1	21.0	41.86
128	2	30	0	1:4	3.8	7.82
129	2	20	55	1:4	17.0	52.33
130	2	20	90	1:4	25.0	75.04
131	2	50	0	4:1	8.8	11.43
132	2	20	55	1:1	17.0	59.25
133	2	30	0	1:1	5.6	11.41
134	2	30	0	4:1	8.4	18.51
135	2	20	90	1:1	20.0	59.28
136	5	50	55	1:1	43.0	51.49
137	5	20	55	1:1	20.0	69.71
138	5	20	0	1:4	3.4	10.47
139	5	30	90	4:1	30.0	59.79
140	5	50	90	1:4	86.0	101.91
141	5	20	90	1:4	20.0	60.03
142	5	50	90	1:1	31.0	37.07
143	5	50	0	1:4	4.8	5.94
144	5	50	0	4:1	6.6	8.57
145	5	20	90	4:1	14.0	42.14
146	5	20	55	4:1	15.0	48.31
147	5	30	0	4:1	4.9	10.80
148	5	50	90	4:1	30.0	36.12
149	5	30	0	1:1	3.6	7.34
150	5	30	55	1:4	21.0	42.60
151	5	30	55	4:1	20.0	40.81
152	5	20	55	1:4	16.0	49.26
153	5	30	90	1:4	25.0	49.88
154	5	50	55	1:4	56.0	68.94
155	5	20	0	1:1	3.4	10.68
156	5	30	55	1:1	16.0	32.64
157	5	20	0	4:1	4.1	13.48
158	5	20	90	1:1	12.0	35.57
159	5	50	0	1:1	5.1	6.39
160	5	30	0	1:4	2.2	4.53
161	5	30	90	1:1	15.0	29.01
162	5	50	55	4:1	29.0	35.07